Electron–Phonon Coupling in Two-Dimensional Superconductors: Doped Graphene and Phosphorene

G. Profeta, C. Tresca and A. Sanna

Abstract The advent of two-dimensional materials with the possibility to vary their physical properties by means of doping, strain, electric, and magnetic fields allows to explore novel physical effects in the two-dimensional limit, where electronic, magnetic, and structural properties can be very different with respect to three-dimensional case. For example, the possibility to synthesize a two-dimensional superconductor will open the doors to new and unexplored applications in present nanotechnology. In this respect, reliable predictions of the superconducting critical temperature from first-principles and in real materials are important prerequisite to make important advances along this line of research. In this work, we review the results of recent theoretical predictions of superconductivity in experimentally realized two-dimensional superconductors: doped graphene and doped phosphorene. And for the latter system, we also present an analysis of several realistic dopants that could induce a superconducting state.

1 Introduction

The discovery of graphene [1], the two-dimensional (2D) allotrope of carbon, has opened the era of 2D system and soon boosted the interest of nanotechnology industry for layered and 2D materials. After the successful isolation of graphene and the measurement of its extraordinary physical properties [2] many other 2D allotrope of layered 3D materials were discovered, *de-facto* establishing a completely new research line in condensed matter physics. Two-dimensional materials can be built with various techniques (molecular beam epitaxy, etching, exfoliation, chemical

G. Profeta (✉) · C. Tresca
Department of Physical and Chemical Sciences, University of L'Aquila,
Via Vetoio 10, 67100 L'aquila, Italy
e-mail: gianni.profeta@aquila.infn.it

G. Profeta · C. Tresca
SPIN-CNR, University of L'Aquila, Via Vetoio 10, 67100 L'aquila, Italy

A. Sanna
Max-Planck-Institut Für Mikrostrukturphysik, Weinberg 2, 06120 Halle, Germany

V. Morandi and L. Ottaviano (eds.), *GraphITA*, Carbon Nanostructures,
DOI 10.1007/978-3-319-58134-7_3

vapor deposition), and designed like nanostripes, junctions, arrays, thin films, etc., giving many new technological applications. One of the most attractive physical properties is represented by the possibility to tune the electron density by means of molecular or atomic dopants, electric field effect, deposition on suitable substrates, etc. As a consequence, it is possible to tune material specific properties to optimal values or induce completely new (quantum) effects exploiting the enhancing of electron correlations in 2D. For example, the possibility to have or induce superconductivity in a 2D material will add a fundamental building block in the future nanotechnology.

Indeed, in recent few years, the frontier of the research in condensed matter physics moved toward the discovery of new and unexpected superconducting (SC) 2D systems. In particular, the research lines are of three types: (i) induce a superconducting phase in a otherwise non-superconducting 2D system by means of charge doping. The most striking example is represented by lithium-doped graphene [3, 4] (see below). The role of the dopants can be twofold: vary the 2D charge density and induce extra pairing channels. (ii) Use the electronic double-layer transistor to induce a charge accumulation at the interface between (insulating) 2D material and the ionic-liquid. For example, in 2010 the group of Iwasa showed [5] able to induce superconductivity in an insulator, ZrNCl. The discovery, made possible by unprecedented technological advances, paved the way to new routes to study, manipulate, and design SC materials and devices making possible, by gating, to realize a 2D metallic state in a single surface layer of any layered semiconducting material. Indeed, the technique has been applied to many transition metal dichalcogenides (TMD), which have been proven to be superconductors with relatively high T_C: MoS_2 ($T_C \approx 10\,K$) [6], WS_2 ($T_C \approx 4\,K$) [7], $MoSe_2$ ($T_C \approx 7\,K$) [8]. The two dimensionality of such system results in peculiar properties like, e.g., the anomalous response of the SC phase to the in-plane magnetic field, probably associated to the spin-orbit coupling and/or valley-dependent Berry curvature [9]. This research field is at the very early stage and new and unexplored phenomena, systems and effects must be highlighted. Interestingly, both the layered materials and the experimental technique are perfectly integrated with the emerging 2D technologies based on graphene and post-graphene materials. (iii) growth of inherently 2D superconducting systems. Notable and recent examples are the discovery of superconductivity in 2D Pb/Si(111) [10] and FeSe monolayer on Nb-doped $SrTiO_3$ (100) substrate [11] at a record $T_C$of 100 K [12].

The field of research is very active, considering that new and promising 2D systems are routinely discovered and synthesized. Moving from carbon (graphene) along the group IV elements the 2D form of silicon (silicene [13]), of germanium (germanene [14]) and tin (stanene [15]) with a buckled graphene-like honeycomb structure, have been observed. Moving along the nearby group V elements the most important example is represented by phosphorene [16], the single layer 2D form of black phosphorous. At the same time, very recently, the 2D form of a single group III element was reported: borophene [17].

The exploration of possible new physical properties of these 2D materials by chemical, field, and interface modification is appealing and represents the ultimate frontier of material science, for both fundamental impact and technological applications.

However, in order to guide the experimental research, propose new materials, predict novel unexpected phenomena, study possible alternative dopants and chemical modifications, a crucial ingredient is a solid, reliable and quantitative predictive, theoretical and computation framework. First-principles density functional theory (DFT) at the moment represents a formidable computational tool to predict (quantitatively) many different materials specific (normal state) properties. In the original practical formulation, expressed by the Kohn–Sham approach [18], the (Gauge breaking) superconducting phase was not explicitly included. This further step can be achieved either by means of many body perturbation theory on top of the non-superconducting Kohn–Sham system, like in the Eliashberg approach [19]; or by means of DFT for superconductors [20] (SCDFT).

Eliashberg theory is the most used theory in ab-initio superconductivity [21], in its general form it is based on the self consistent solution of a Dyson-like equations for the Nambu Green's function [22], and allows to compute the most relevant experimental observables in superconductors [23]. A large literature is devoted to its development including anisotropy, multiband effects, non-adiabaticity, and more [24–27]. However, especially to obtain a quick estimation of the superconducting T_C Eliashberg theory is often used in a parameterized form, like the one obtained by McMillan [28].

An alternative to Eliashberg theory is SCDFT [20] that is a generalization of DFT to include the effect of a superconducting symmetry breaking. First developed for phononic superconductors [29] it was more recently extended to other pairing channels [30, 31]. SCDFT has been applied to the study of elemental superconductors [32, 33] and alloys like MgB_2 [34, 35], CaC_6 [36], intercalated graphites [37], high pressure hydrides [38, 39]. At the same time, the first-principles nature of the theory and the possibility to describe real materials (not only models) allowed prediction of superconducting properties of new materials: high temperature superconductivity of hydrogen under high pressure [40–42], CaBeSi [43], potassium under pressure [44, 45].

The advantage of SCDFT with respect to Eliashberg theory is its lower computational cost and the possibility of full ab-initio inclusion of the Coulomb interaction that makes it completely parameter free. On the contrary Eliashberg's theory has the advantage of being directly formulated in terms of Feynman diagrams, therefore it does not require the cumbersome step of the functional construction that is usually the bottleneck for the development of density functional methods.

Nowadays, the superconducting critical temperature can be quantitatively predicted by first-principles DFT calculations, and can even anticipate and guide experiments in the discovery of new superconductors [46, 47]. The aim of this paper is to review first-principles DFT predictions of normal and superconducting state physical properties of new 2D materials. In order to have a widespread look of the state of

the art, we review results on theoretical predictions of superconductivity in graphene, recently confirmed by the experiments on the metallization of phosphorene to induce a superconducting phase.

2 Superconducting Graphene

The possibility to turn graphene into a superconductor is a fascinating research area which involved many different approaches, both experimentally than theoretically.

A first attempt by the Morpurgo's group in 2007 [48] used a Josephson effect between graphene and superconducting electrodes which demonstrated that graphene can support supercurrents. The theoretical proposal has focused on electron correlation driven superconductivity in doped graphene [49] due to the very low electron–phonon coupling in graphene. Indeed, conventional superconductivity, although desirable, was not expected in pure graphene, mainly due to low density of states at the Fermi level on the Dirac bands and the high frequencies of the bond stretching modes. In 2012, a theoretical work, inspired by the physics of graphite intercalated compounds [3] proposed lithium doping of graphene as a possible viable way to observe a superconducting phase at relatively high temperatures. The main idea was founded on the possibility to promote the so-called interlayer band (present in pure graphene at very high energies) at the Fermi energy by means of positive potential of the ionized lithium adatoms. Indeed, at a coverage of 1 Li per 6 C atoms (LiC_6 stoichiometry), lithium induces a $\sqrt{3} \times \sqrt{3}R30°$ ($\sqrt{3}$) in-plane unit cell (with respect to a standard graphene lattice) with one adatom per unit cell, adding an additional (with respect to linear Dirac bands) band at the Fermi energy (see Fig. 1). The presence of the interlayer band enhances the electron–phonon coupling, in particular at low frequency modes where the contribution to the total electron–phonon coupling (λ) is more effective. The low energy phonons are mainly characterized by out-of-

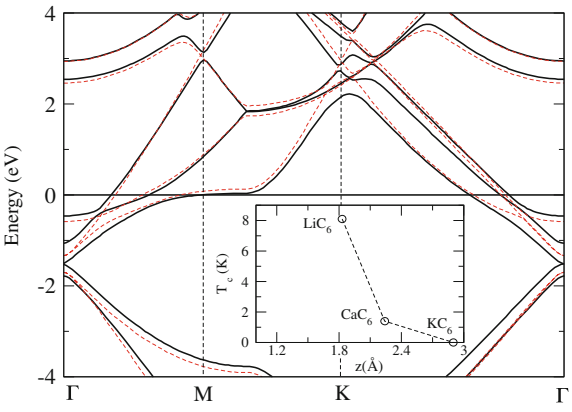

Fig. 1 Band structure of lithium-doped graphene in the $\sqrt{3}$ phase in the equilibrium configuration (*red dashed curve*) and with carbon atoms displaced along the B_{2g} phonon mode at the Γ-point (*solid black curve*)

plane displacements of carbon atoms which couples with the electrons occupying the interlayer band and localized around lithium atoms [50, 51]. Indeed, by symmetry in graphene the relevant out-of-plane phonons (B_{2g}) have the same symmetry as the π^* electronic states. Upon adatom deposition, lithium in this case, the symmetry argument is not more valid, and the coupling with B_{2g} phonons becomes possible. The electron–phonon matrix element M_i^j for the band j coupling with optical mode i can be obtained by:

$$M_j^i = \sqrt{\frac{\hbar}{2MN\omega^i}} \sum_a \epsilon_a^i \frac{\partial E_j(\mathbf{k})}{\partial \mathbf{u_a}}$$

where a denotes the atom in the unit cell, $\mathbf{k}$ and j correspond to the wavevector and band index of the electronic state. M is the atomic mass, and $\mathbf{u}_a$ is the normalized polarization eigenvector of the phonon. In order to understand the electron–phonon coupling between π states and the Γ-point B_{2g} phonons, we calculated the deformation potential, $D = \frac{\partial E_j(\mathbf{k})}{\partial \mathbf{u_a}}$, at the Γ point of π states, distorting C atoms of graphene by u along the B_{2g} phonon eigenvector and calculating of the energy shift (ΔE) between π and π^* states. We performed first-principles DFT calculation in the local density approximation [52]. The QUANTUM-ESPRESSO [53] package was used with norm-conserving pseudopotentials and a plane-wave cutoff energy of 65 Ry. All of the structures considered were relaxed to their minimum energy configuration following the internal forces on atoms and the stress tensor of the unit cell. The monolayer systems were simulated in the $\sqrt{3} \times \sqrt{3}R30°$ in-plane unit cell (with respect to a standard graphene lattice) with one adatom per unit cell [3]. In Fig. 1, we report the band structure of LiC_6 with and without the phonon deformation.

It is evident that the out-of-plane phonon mode activate a relevant splitting of both π and π^* bands giving a deformation potential of $D = 5.2$ eV/Å. Considering that the square of the electron–phonon matrix elements enters in the definition of λ it results a relevant term.

This is the most evident manifestation of the increased electron–phonon coupling in graphene, due to the adsorption of lithium adatoms. Evidently the coupling between out-of-plane B_{2g} modes depends on the distance between adatom and graphene layers. We demonstrate this aspect, calculating the superconducting critical temperature for other two prototype systems, namely: calcium on graphene (CaC_6) and potassium on graphene (KC_6). Both systems have been simulated in the same $\sqrt{3} \times \sqrt{3}R30°$ of LiC_6. The different ionic radius (r) of the adatoms ($r_{Li} = 0.8$ Å, $r_{Ca} = 1.0$ Å and $r_K = 1.4$ Å) determines a different adsorption height above the graphene layers, changing the electron–phonon coupling and the relative T_C. In the inset of Fig. 1, we report the critical temperature as a function of the equilibrium height. The calculation confirms that the critical temperature strongly increased reducing the adatom/graphene distance which influences the electron–phonon coupling with B_{2g} modes.

The theoretical proposal of a possible superconducting phase in lithium-doped graphene was recently put on a real ground by the Damascelli's group [4] which demonstrated that lithium decorated graphene presents a superconducting phase with a critical temperature of 5.9 K. The measured critical temperature is in line with the theoretical prediction giving a strong indication that the observed crystal phase is indeed the theoretical proposed $\sqrt{3} \times \sqrt{3}R30°$. One of the main indication of the formation of the superstructure is the folding of the π bands from the K-point of the graphene unit cell to the Γ-point of the $\sqrt{3}$ Brillouin zone. This last evidence ensures the presence of the interlayer state crossing the Fermi level which strongly contributes to the increase of the electron–phonon coupling [54]. In Ref. [4], the authors measured the Γ-point intensity of the spectral weight as a function of the deposition time, revealing the presence of the Li-2s band expected for this system [3] superimposed with the folded graphene bands caused by a Li superstructure, which were observed in Li and Ca bulk GIC systems [54, 55]. This spectral weight, which disappears above $\simeq$50 K and is not recovered on subsequent cooling, is associated with the strong enhancement of electron–phonon coupling.

In Fig. 3E of Ref. [4], the Fermi surface of Li-doped system is reported. This represents an important experimental evidence: its comparison with first-principles theoretical prediction will represent a strong fingerprint of the realization of the $\sqrt{3}$, superconducting, phase. In Fig. 2 we report Fig. 1E of Ref. [4] superimposed with calculated Fermi surface of the Li/graphene structure in the $\sqrt{3}$ phase. The agreement between the theoretical and experimental Fermi surfaces is excellent, in particular considering the low spectral weight of the interlayer state. The notable agreement in the size of the Fermi surface indicates that the doping level reached in the experiments is exactly what predicted for the $\sqrt{3}$ phase.

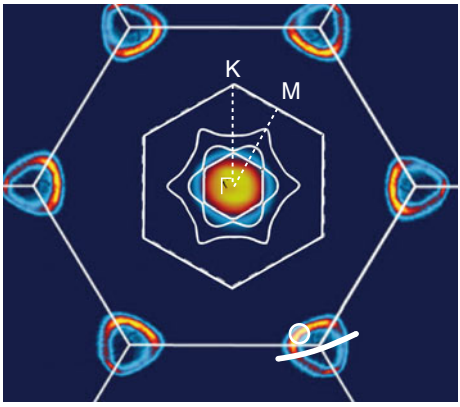

Fig. 2 Experimental (taken from Fig. 1E of Ref. [4]) and theoretical Fermi surface (*white solid line*). The large hexagonal Brillouin zone represents the 1×1 graphene BZ, while the inner hexagonal BZ (rotated by 30° with respect to the first one) is the $\sqrt{3}$ BZ of the lithium-doped graphene

We conclude this section summarizing the theoretical results obtained for the superconducting $\sqrt{3}$ phase of lithium-doped graphene: (i) we demonstrate that lithium deposition activate the electron–phonon coupling between B_{2g} out-of-plane modes which induces a sizable splitting of the π bands. (ii) comparison between experimental and theoretical Fermi surfaces at the Γ point reveals an excellent agreement for the interlayer Fermi surface, indicating that the experimental procedure adopted in Ref. [4] indeed produced a $\sqrt{3}$ phase.

3 Metallic Phosphorene: A Novel Superconducting 2D Material

The successful isolation of graphene [1], demonstrated the possibility of use three-dimensional materials in which different layers are brought together by weak van der Waals forces as prototype system for growth of different 2D systems [56]. Indeed, in the last few years, it has been discovered that many different layered bulk materials, like graphite, hexagonal boron nitrite, transition metal dichalcogenides, and iron-chalcogenides [11], posses stable single layer allotropes. These have been obtained experimentally by many different growth methods and represent building blocks of new and possibly useful functional materials. Recently, another member of this family was discovered by means of mechanical exfoliation: the few layer phosphorene[16] was reported and plasma-assisted fabrication [57] allowed the fabrication of the first transistor of single layer black phosphorus [58]. The physical and chemical properties of few layer black phosphorus and its single layer form, phosphorene, are very promising so that they can be considered for nanoelectronic and nanophotonic applications [59]. They combine high electron mobilities like in graphene [58] with the existence of a direct moderate band gap (∼0.3 eV) (in between graphene and transition metal dichalcogenides insulators) which is strongly dependent on the number of layers [60, 61] and strain conditions [62]. Although the semiconducting properties of phosphorene and black phosphorus are so appealing, electron and hole doping represents an important possibility to tune the physical properties and device applications. In principle, doping can be achieved by gating, using an electrolyte gate [63], or by charge-transfer doping as demonstrated in other 2D systems like graphene [64] and MoS_2 [65]. Black phosphorous is completely unexplored in this aspect posing the important question whether it could be functionalized as most of the other 2D materials known. Moreover, charge doping can induce new and unexpected physical properties. For example, superconductivity, one of the most striking phenomena in nature, was recently induced in many 2D systems using suitable substrates [11], electric field [6] and chemical doping [3]. This last possibility is particular appealing considering that moderate doping of 2D semiconductors can result in relatively large superconducting critical temperatures [66]. In this section, we study, by first-principles calculations, the metallization of phosphorene surface by means of metal deposition which moves the Fermi level into the conduction band.

We further explored the effects of the charge doping on the electron–phonon coupling (EPC) predicting a possible superconducting phase of electron and hole doped phosphorene.

3.1 Computational Methods

We performed first-principles DFT calculations within Kohn–Sham local density approximation using norm conserving pseudopotentials, as implemented in the ESPRESSO package [53]. To model a single phosphorene layer, we considered a vacuum space of 15 Å between the periodic replicas. Results are converged using 58 Ry of plane-wave cutoff and a 14×14 uniform k-point grid for charge density integration. We relaxed both lattice constants and internal structural parameters in the lowest energy configuration. Phonon and electron–phonon coupling have been calculated within the Linear Response Theory [53] on a 10×10 phonon q-grid as referred to the undoped unit cell. Supercells are computed with equivalent grids. The superconducting critical temperature was estimated within Eliashberg theory in form of the Allen–Dynes parameterization [22, 67]:

$$T_C = f_1 f_2 \frac{\omega_{\log}}{1.2 k_B} \exp\left[\frac{-1.04\,(1+\lambda)}{\lambda - \mu^*\,(1+0.62\lambda)}\right] \tag{1}$$

where k_B is the Boltzmann constant and μ^* the Morel–Anderson pseudopotential [21, 68]. λ and $\omega_{\log}$ are, respectively, the electron–phonon coupling parameter and a logarithmic phonon average, defined as

$$\lambda = 2 \int \frac{\alpha^2 F(\omega)}{\omega} d\omega \tag{2}$$

$$\omega_{\log} = \exp\left[\frac{2}{\lambda} \int \frac{\ln(\omega)}{\omega} \alpha^2 F(\omega) d\omega\right] \tag{3}$$

by means of the Eliashberg function $\alpha^2 F(\omega)$ [19, 22, 23]. The two prefactors f_1 and f_2 are an important correction to the original McMillan form [28], and make Eq. 1 significantly more accurate. They read:

$$f_1 = \left\{1 + \left[\lambda / 2.46\,(1 + 3.8\mu^*)\right]^{3/2}\right\}^{1/3} \tag{4}$$

$$f_2 = \frac{1 + \lambda^2 \left(\omega_2/\omega_{\log} - 1\right)}{\lambda^2 + 3.31\,(1 + 6.3\mu^*)^2\, \omega_2/\omega_{\log}},$$

where

$$\omega_2 = \left[\frac{2}{\lambda}\int \omega\alpha^2 F(\omega)d\omega\right]^{1/2}. \quad (5)$$

3.2 Rigid Shift Doping

The band structure of a single phosphorene layer is reported as a reference in Fig. 3. Phosphorene is a semiconductor with the top of the valence band (Γ) characterized by a $p_z p_z$ bonding combination while the bottom of the conduction band is of an anti-bonding nature. The undoped system is insulating with a direct band gap at Γ of 0.5 eV in LDA (Fig. 3).

We studied the EPC in phosphorene monolayer and give a possible experimental way to dope the covalent $p_z p_z$ anti-bonding states, making the system metallic. The EPC and its variation with charge doping was studied as a function of the Fermi energy from negative (hole doping) to positive values (electron doping), by a rigid shifting of the Fermi energy considering the phonon frequencies calculated in the undoped (insulating) system. The behavior of the critical temperature as a function

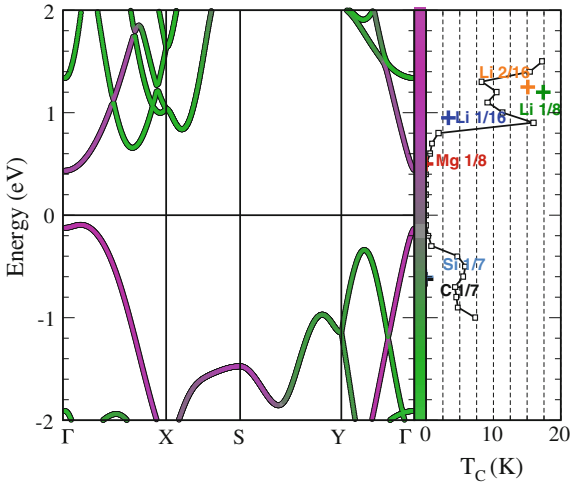

Fig. 3 *Left panel* Kohn–Sham LDA band structure of undoped (insulating) phosphorene. The color-scale (*green* to *violet*) is proportional to the P-p_z character of the KS-state. *Right panel* estimation of the superconducting critical temperature (see text) as a function of the Fermi level position. The zero of the energy represents the valence band maximum of the undoped phosphorene. Points and labels represent the critical temperature obtained considering the inclusion of dopants (see text)

of doping is reported in the right panel of Fig. 3. A maximum T_C of the order of 15 K can be achieved moving the Fermi level at $\simeq$0.5 eV above the conduction band minimum. Hole doping, on the contrary should be less promising. The estimated relevant superconducting critical temperatures upon electron doping deserves further investigations, in particular considering a more detailed and realistic system including dopant atoms. In fact, a rigid shift doping picture does not account either for the local distortion that real doping will induce or, most important, for the screening of phonons when the system becomes metallic [69], and therefore does not consider the possibility of a dynamical instability induced by the doping.

3.3 Realistic Doping by Intercalation or Adsorption

To achieve a more reliable estimation of the superconducting properties of doped phosphorene, we have extended our calculations by simulating real doping by foreign atoms: Si, C, Mg, Li. In particular, lithium doping was simulated at different concentration in order to assess the effect of coverage on the final superconducting critical temperature.

We have used a simulation supercell containing 8 P atoms/unit cell and one substitutional (for hole dopants, Si and C) or adsorbed (for electron dopants, Mg, and Li). While to study lower concentration (1/16) of lithium doping and a different lithium absorption geometry (one lithium atom on both sides of phosphorene layer) we have used a doubled supercell containing 16 P atoms. A sketch of the simulation cells and dopings is shown in the upper panel of Fig. 4. The same figure also shows the calculated α^2F functions. These are used within Eliashberg theory (Allen–Dynes formula of Eq. 1, assuming a $\mu^* = 0.1$) to estimate the superconducting critical temperature.

In Table 1, we report a summary of the relevant parameters which set the superconducting critical temperature for the different systems we considered. As evident, hole dopants (Si and C), in line with estimation based on rigid band approach, do not induce a superconducting phase at relevant critical temperatures. The density of states at the Fermi energy is rather low and so is the integrated coupling λ. On the contrary, electron doping, in particular lithium doping, gives an appreciable superconducting critical temperature with a predicted $T_C = 17.5$ K at 1/8 of coverage. Reducing doping (1/16), or doping on both sides of phosphorene (2/16), decreases the critical temperature. We include the calculated T_C with the rigid doping estimation in Fig. 3. Some considerations are important: although rigid doping effectively gives a good indication that electron–doping is more effective of hole doping to have higher critical temperatures, the quantitative estimation cannot be reliable. The effect of local interaction between different atoms and phosphorene results in different dynamical and electronic properties which cannot be accounted by simple rigid doping. A clear evidence for this effect is given by the inspection of the spectral structure of the $\alpha^2F(\omega)$ for the different systems (see Fig. 4).

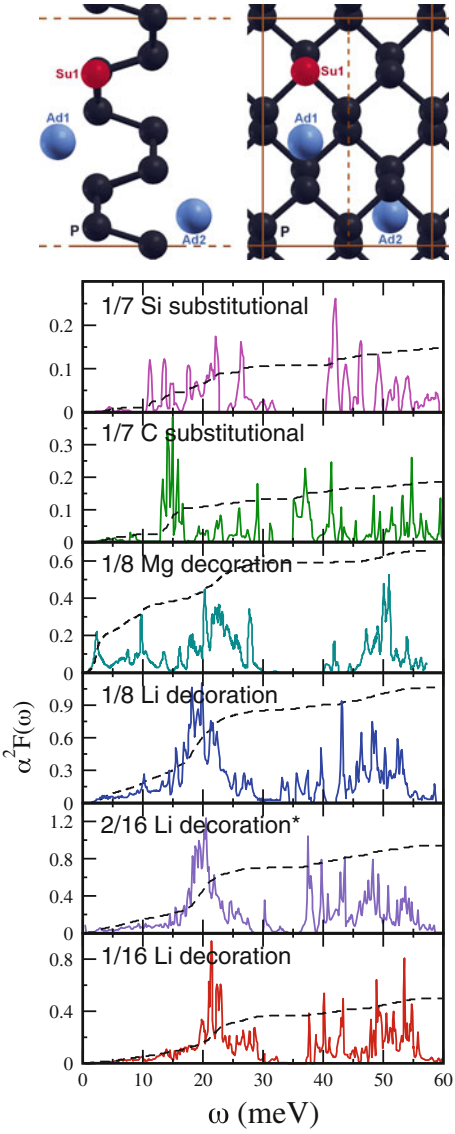

Fig. 4 *Top*: simulation cell of doped phosphorene, side view (*left*) and top view (*right*). The large unit cell (*full orange lines*) contains 16 P atoms, while the smaller one (limited by the *dashed orange line*) contains 8 atoms. Substitutional position (Su1) is shown as a *red dot*. Surface adsorbed positions (Ad1 and Ad2) are shown as *light blue dots*. In the smaller simulation cell we have considered Si and C doping in Su1 and Mg and Li doping in Ad1. In the larger simulation cell a single Li doping in Ad1 and a double Li doping in Ad1 and Ad2. *Bottom*: Eliashberg functions: $\alpha^2F(\omega)$. *Dashed curves* represent $\lambda(\omega) = 2\int_0^{\omega} \frac{\alpha^2F(\omega')}{\omega'} d\omega'$. The label of different systems are consistent with that of Table 1

The origin of the high electron–phonon coupling in lithium-doped systems resides on the increase of the spectral weight in the region of 15–30 (meV), characterized by out-of-plane vibrations [70] of phosphorene. On the contrary, both Si and C are strongly detrimental for the electron–phonon coupling at all the frequencies, while Mg results in a lower coupling due to the higher distance from the phosphorene layer, which reduces the coupling with out-of-plane modes (in line with what observed in graphene). The overall coupling strength of the Mg system is actually high ($\lambda = 0.65$)

Table 1 Couplings and critical temperatures of doped phosphorene systems. λ is the electron–phonon coupling (Eq. 2), ω_{rmlog} the logarithmic averaged (Eq. 3) characteristic frequency (in meV) of the Eliashberg function [22]. T_C is the critical temperature (in K) computed with Eq. 1 and assuming $\mu^* = 0.1$. $N(E_F)$ is the density of states at the Fermi lever (in states/eV/spin). Si and C dopings are substitutional, dopings on a 8 atoms supercell. Mg and Li dopings are decorations of the phosphorene surface. 1/8 dopings are performed on a phosphorene supercell containing 8 P atoms. While 1/16 and 2/16 are performed on a supercell with 16 P atoms. The 2/16 system is decoration is done on both faces of the phosphorene monolayer

	λ	ω_{rmlog}	T_C	$N(E_F)$
1/7 Si	0.14	12.0	0.0	0.35
1/7 C	0.20	20.3	0.0	0.5
1/8 Mg	0.65	8.8	3.2	0.95
1/8 Li	1.06	17.5	17.4	2.12
2/16 Li*	1.00	15.1	13.8	3.78
1/16 Li	0.50	21.7	3.31	1.65

however, as seen in Fig. 4 this is due to an incipient phononic instability (low energy peak in the α^2F function), however this peak pushes down the logarithmic average of the same function, and with this T_C [22, 67].

4 Conclusions

We have presented first-principles DFT calculations of the electron–phonon coupling properties of doped 2D systems, graphene and phosphorene, underling the main physical mechanisms which sets the superconducting critical temperature. In graphene, the presence of an interlayer band at the Fermi energy is responsible for the increased electron–phonon coupling as confirmed in recent experiments [4]. The comparison between experimental and theoretical Fermi surfaces, indeed confirmed that the superconducting phase is characteristic of the $\sqrt{3}$ surface reconstruction. On the contrary, lithium induces a metallic phase in semiconducting phosphorene. Filling the covalent antibonding p_z states of phosphorous and increasing the density of states at the Fermi energy, lithium makes phosphorene superconducting with a predicted $T_C = 17.5$ K.

We underline that both theoretical predictions were experimentally confirmed: graphene was found superconducting with critical temperature of the order of the predicted one [4], while the possibility to effectively dope phosphorene into a metallic phase was recently demonstrated by ARPES experiments [70].

Acknowledgements G.P. acknowledges support by the Supercomputing center Cineca (Bologna, Italy) through ISCRA projects.

References

1. Novoselov, K.S., Geim, A.K., Morozov, S.V., Jiang, D., Zhang, Y., Dubonos, S.V., Grigorieva, I.V., Firsov, A.A.: Science **306**, 666 (2004)
2. Castro Neto, A.H., Guinea, F., Peres, N.M.R., Novoselov, K.S., Geim, A.K.: Rev. Mod. Phys. **81**, 109 (2009)
3. Profeta, G., Calandra, M., Mauri, F.: Nat. Phys. **8**, 131 (2012)
4. Ludbrook, B.M., Levy, G., Nigge, P., Zonno, M., Schneider, M., Dvorak, D.J., Veenstra, C.N., Zhdanovich, S., Wong, D., Dosanjh, P., Straer, C., Sthr, A., Forti, S., Ast, C.R., Starke, U., Damascelli, A.: Proc. Nat. Acad. Sci. **112**, 11795 (2015). http://www.pnas.org/content/112/38/11795.full.pdf
5. Ye, J.T., Inoue, S., Kobayashi, K., Kasahara, Y., Yuan, H.T., Shimotani, H., Iwasa, Y.: Nat. Mater. **9**, 125 (2010)
6. Ye, J.T., Zhang, Y.J., Akashi, R., Bahramy, M.S., Arita, R., Iwasa, Y.: Science **338**, 1193 (2012)
7. Jo, S., Costanzo, D., Berger, H., Morpurgo, A.F.: Nano Lett. **15**, 1197 (2015), pMID: 25607653. doi:10.1021/nl504314c
8. Shi, W., Ye, J., Zhang, Y., Suzuki, R., Yoshida, M., Miyazaki, J., Inoue, N., Saito, Y., Iwasa, Y.: Sci. Rep. **5**, 12534 (2015)
9. Lu, J.M., Zheliuk, O., Leermakers, I., Yuan, N.F.Q., Zeitler, U., Law, K.T., Ye, J.T.: Science **350**, 1353 (2015). http://science.sciencemag.org/content/350/6266/1353.full.pdf
10. Zhang, T., Cheng, P., Li, W.-J., Sun, Y.-J., Wang, G., Zhu, X.-G., He, K., Wang, L., Ma, X., Chen, X., Wang, Y., Liu, Y., Lin, H.-Q., Jia, J.-F., Xue, Q.-K.: Nat. Phys. **6**, 104 (2010)
11. Qing-Yan, W., Zhi, L., Wen-Hao, Z., Zuo-Cheng, Z., Jin-Song, Z., Wei, L., Hao, D., Yun-Bo, O., Peng, D., Kai, C., Jing, W., Can-Li, S., Ke, H., Jin-Feng, J., Shuai-Hua, J., Ya-Yu, W., Li-Li, W., Xi, C., Xu-Cun, M., Qi-Kun, X.: Chin. Phys. Lett. **29**, 037402 (2012)
12. Ge, J.-F., Liu, Z.-L., Liu, C., Gao, C.-L., Qian, D., Xue, Q.-K., Liu, Y., Jia, J.-F.: Nat. Mater. **14**, 285 (2015)
13. Tao, L., Cinquanta, E., Chiappe, D., Grazianetti, C., Fanciulli, M., Dubey, M., Molle, A., Akinwande, D.: Nat. Nano **10**, 227 (2015)
14. Dvila, M.E., Xian, L., Cahangirov, S., Rubio, A., Lay, G.L.: New J. Phys. **16**, 095002 (2014)
15. Zhu, F.-F., Chen, W.-J., Xu, Y., Gao, C.-L., Guan, D.-D., Liu, C.-H., Qian, D., Zhang, S.-C., Jia, J.-F.: Nat. Mater. **14**, 1020 (2015)
16. Li, L., Yu, Y., Ye, G.J., Ge, Q., Ou, X., Wu, H., Feng, D., Chen, X.H., Zhang, Y.: Nat. Nano **9**, 372 (2014)
17. Mannix, A.J., Zhou, X.-F., Kiraly, B., Wood, J.D., Alducin, D., Myers, B.D., Liu, X., Fisher, B.L., Santiago, U., Guest, J.R., Yacaman, M.J., Ponce, A., Oganov, A.R., Hersam, M.C., Guisinger, N.P.: Science **350**, 1513 (2015). http://science.sciencemag.org/content/350/6267/1513.full.pdf
18. Kohn, W., Sham, L.J.: Phys. Rev. **140**, A1133 (1965)
19. Eliashberg, G.: J. Exptl. Theor. Phys. (U.S.S.R.) 11, 966, : Sov. Phys. JETP **38**, 696 (1960)
20. Oliveira, L.N., Gross, E.K.U., Kohn, W.: Phys. Rev. Lett. **60**, 2430 (1988)
21. Scalapino, D.J., Schrieffer, J.R., Wilkins, J.W.: Phys. Rev. **148**, 263 (1966)
22. Allen, P.B., Mitrović, B.: Solid State Phys. **37** (1960)
23. Carbotte, J.P.: Rev. Modern Phys. **62**, 1027 (1990)
24. Margine, E.R., Giustino, F.: Phys. Rev. B **87**, 024505 (2013)
25. Sanna, A., Pittalis, S., Dewhurst, J.K., Monni, M., Sharma, S., Ummarino, G., Massidda, S., Gross, E.K.U.: Phys. Rev. B **85**, 184514 (2012)
26. Pietronero, L., Strässler, S., Grimaldi, C.: Phys. Rev. B **52**, 10516 (1995)
27. Grimaldi, C., Pietronero, L., Strässler, S.: Phys. Rev. B **52**, 10530 (1995)
28. McMillan, W.L.: Phys. Rev. **167**, 331 (1968)
29. Lüders, M., Marques, M.A.L., Lathiotakis, N.N., Floris, A., Profeta, G., Fast, L., Continenza, A., Massidda, S., Gross, E.K.U.: Phys. Rev. B **72**, 024545 (2005)
30. Essenberger, F., Sanna, A., Linscheid, A., Tandetzky, F., Profeta, G., Cudazzo, P., Gross, E.K.U.: Phys. Rev. B **90**, 214504 (2014)

31. Akashi, R., Arita, R.: Phys. Rev. Lett. **111**, 057006 (2013)
32. Marques, M.A.L., Lüders, M., Lathiotakis, N.N., Profeta, G., Floris, A., Fast, L., Continenza, A., Gross, E.K.U., Massidda, S.: Phys. Rev. B **72**, 024546 (2005)
33. Floris, A., Sanna, A., Massidda, S., Gross, E.K.U.: Phys. Rev. B **75**, 054508 (2007)
34. Floris, A., Profeta, G., Lathiotakis, N.N., Lüders, M., Marques, M.A.L., Franchini, C., Gross, E.K.U., Continenza, A., Massidda, S.: Phys. Rev. Lett. **94**, 037004 (2005)
35. Linscheid, A., Sanna, A., Floris, A., Gross, E.K.U.: Phys. Rev. Lett. **115**, 097002 (2015)
36. Sanna, A., Profeta, G., Floris, A., Marini, A., Gross, E.K.U., Massidda, S.: Phys. Rev. B **75**, 020511 (2007)
37. Flores-Livas, J.A., Sanna, A.: Phys. Rev. B **91**, 054508 (2015)
38. Flores-Livas, J.A., Sanna, A., Gross, E.K.U.: Eur. Phys. J. B **89**, 63 (2016)
39. Flores-Livas, J.A., Amsler, M., Heil, C., Sanna, A., Boeri, L., Profeta, G., Wolverton, C., Goedecker, S., Gross, E.K.U.: Phys. Rev. B **93**, 020508 (2016)
40. Cudazzo, P., Profeta, G., Sanna, A., Floris, A., Continenza, A., Massidda, S., Gross, E.K.U.: Phys. Rev. Lett. **100**, 257001 (2008)
41. Cudazzo, P., Profeta, G., Sanna, A., Floris, A., Continenza, A., Massidda, S., Gross, E.K.U.: Phys. Rev. B **81**, 134505 (2010)
42. Cudazzo, P., Profeta, G., Sanna, A., Floris, A., Continenza, A., Massidda, S., Gross, E.K.U.: Phys. Rev. B **81**, 134506 (2010)
43. Bersier, C., Floris, A., Sanna, A., Profeta, G., Continenza, A., Gross, E.K.U., Massidda, S.: Phys. Rev. B **79**, 104503 (2009)
44. Sanna, A., Franchini, C., Floris, A., Profeta, G., Lathiotakis, N.N., Lüders, M., Marques, M.A.L., Gross, E.K.U., Continenza, A., Massidda, S.: Phys. Rev. B **73**, 144512 (2006)
45. Profeta, G., Franchini, C., Lathiotakis, N.N., Floris, A., Sanna, A., Marques, M.A.L., Läders, M., Massidda, S., Gross, E.K.U., Continenza, A.: Phys. Rev. Lett. **96**, 047003 (2006)
46. Drozdov, A.P., Eremets, M.I., Troyan, I.A., Ksenofontov, V., Shylin, S.I.: Nature **000** (2015)
47. Duan, D., Liu, Y., Tian, F., Li, D., Huang, X., Zhao, Z., Yu, H., Liu, B., Tian, W., Cui, T.: Sci. Rep. **4** (2014). doi:10.1038/srep06968
48. Heersche, H.B., Jarillo-Herrero, P., Oostinga, J.B., Vandersypen, L.M.K., Morpurgo, A.F.: Nature **446**, 56 (2007)
49. Pathak, S., Shenoy, V.B., Baskaran, G.: Phys. Rev. B **81**, 085431 (2010)
50. Calandra, M., Mauri, F.: Phys. Rev. B **74**, 094507 (2006)
51. Boeri, L., Bachelet, G.B., Giantomassi, M., Andersen, O.K.: Phys. Rev. B **76**, 064510 (2007)
52. Perdew, J.P., Zunger, A.: Phys. Rev. B **23**, 5048 (1981)
53. Giannozzi, P., Baroni, S., Bonini, N., Calandra, M., Car, R., Cavazzoni, C., Ceresoli, D., Chiarotti, G.L., Cococcioni, M., Dabo, I., Corso, A.D., de Gironcoli, S., Fabris, S., Fratesi, G., Gebauer, R., Gerstmann, U., Gougoussis, C., Kokalj, A., Lazzeri, M., Martin-Samos, L., Marzari, N., Mauri, F., Mazzarello, R., Paolini, S., Pasquarello, A., Paulatto, L., Sbraccia, C., Scandolo, S., Sclauzero, G., Seitsonen, A.P., Smogunov, A., Umari, P., Wentzcovitch, R.M.: J. Phys. Condens. Matter **21**, 395502 (2009)
54. Yang, S.-L., Sobota, J.A., Howard, C.A., Pickard, C.J., Hashimoto, M., Lu, D.H., Mo, S.-K., Kirchmann, P.S., Shen, Z.-X.: Nat. Commun. **5** (2014)
55. Sugawara, K., Sato, T., Takahashi, T.: Nat. Phys. **5**, 40 (2009)
56. Geim, A.K., Grigorieva, I.V.: Nature **499**, 419 (2013)
57. Lu, W., Nan, H., Hong, J., Chen, Y., Zhu, C., Liang, Z., Ma, X., Ni, Z., Jin, C., Zhang, Z.: Nano Res. **7**, 853 (2014)
58. Liu, H., Neal, A.T., Zhu, Z., Luo, Z., Xu, X., Tománek, D., Ye, P.D.: ACS Nano **8**, 4033 (2014), pMID: 24655084
59. Youngblood, N., Chen, C., Koester, S.J., Li, M.: Nat. Photon **9**, 247 (2015)
60. Tran, V., Soklaski, R., Liang, Y., Yang, L.: Phys. Rev. B **89**, 235319 (2014)
61. Cai, Y., Zhang, G., Zhang, Y.-W.: Sci. Rep. **4**, 6677 EP (2014)
62. Fei, R., Yang, L.: Nano Lett. **14**, 2884 (2014), pMID: 24779386
63. Das, A., Pisana, S., Chakraborty, B., Piscanec, S., Saha, S.K., Waghmare, U.V., Novoselov, K.S., Krishnamurthy, H.R., Geim, A.K., Ferrari, A.C., Sood, A.K.: Nat. Nano **3**, 210 (2008)

64. Fedorov, A.V., Verbitskiy, N.I., Haberer, D., Struzzi, C., Petaccia, L., Usachov, D., Vilkov, O.Y., Vyalikh, D.V., Fink, J., Knupfer, M., Büchner, B., Grüneis, A.: Nat. Commun. **5** (2014)
65. Miwa, J.A., Ulstrup, S., Sørensen, S.G., Dendzik, M., Antonija, G., Bianchi, M., Lauritsen, J.V., Hofmann, P.: Phys. Rev. Lett. **114**, 046802 (2015)
66. Calandra, M., Zoccante, P., Mauri, F.: Phys. Rev. Lett. **114**, 077001 (2015)
67. Allen, P.B., Dynes, R.C.: Phys. Rev. B **12**, 905 (1975)
68. Morel, P., Anderson, P.W.: Phys. Rev. **125**, 1263 (1962)
69. Baroni, S., de Gironcoli, S., Dal Corso, A., Giannozzi, P.: Rev. Mod. Phys. **73**, 515 (2001)
70. Sanna, A., Fedorov, A.V., Verbitskiy, N., Fink, J., Krellner, C., Petaccia, L., Chikina, A., Usachov, D., Grüneis, A., Profeta, G.: submitted (2016)